PERGAMON

Available online at www.sciencedirect.com

SCIENCE DIRECT®

International Journal of Impact Engineering 28 (2003) 349–362

INTERNATIONAL JOURNAL OF IMPACT ENGINEERING

www.elsevier.com/locate/ijimpeng

A numerical study on the detonation behaviour of double reactive cassettes by impacts of projectiles with different nose shapes

Hyunho Shin*, Woong Lee

Ground Systems Development Centre, Agency for Defence Development, P.O. Box 35-1, Yuseong, Daejeon 305-600, South Korea

Received 20 May 2002; received in revised form 8 August 2002

Abstract

The detonation behaviours of two layers of reactive cassettes by the impact of cylindrical steel projectiles with different nose shapes were numerically simulated at 1800 m s^{-1} based on the forest fire explosive reaction rate model. When a projectile with a flat-ended nose impacted the target, a run distance-induced detonation took place at the bulk of the first cassette. In the case of a cone-ended projectile impact, however, a back plate-assisted detonation took place via the superposition of incident and reflective shock waves at the region near the back plate of the first cassette. Since such a mechanism was not observable in the conventional critical initiation criteria (CIC) test, the previously developed CIC models were suggested to be inadequate to predict the detonation sensitivity of a reactive cassette. When a hemispherically nosed projectile impacted the target, none of the detonation mechanisms were triggered, resulting in the failure of detonation. The detonation of the second reactive cassette was not directly influenced by the impact shock of the projectile, but it was achieved only when the first cassette was successfully detonated thereby transferring sufficient energy to the second one.

Keywords: Detonation; Reactive cassette; Explosive reactive armour; Critical initiation criteria; Forest fire model

1. Introduction

Predicting detonation or non-detonation of an explosive when it is impacted by a high-velocity projectile is of great importance in the areas such as warhead design, hazard assessment, storage

*Corresponding author.
E-mail address: shinh@unitel.co.kr (H. Shin).

0734-743X/02/$ - see front matter
PII: S0734-743X(02)00074-X

of munitions, safety and lethality considerations [1,2], and operation of an explosive reactive armour (ERA) [3]. The response reliability of an explosive can be judged in terms of its sensitivity to the external impact which is quantified by the threshold velocity of a projectile to detonate the explosive. The threshold velocity is measured by a methodology known as critical initiation criteria (CIC) test. Fig. 1(a) shows a schematic diagram for the CIC test. In the test, in general, the explosive is freely suspended in space with a free rear surface and a small calibre kinetic energy projectile is impacted onto either bare or front-covered high explosive surface [4–6]. The thickness of the explosive in the CIC test is in general comparable or larger than its lateral dimension [4–7] to ensure a sufficient run distance for an impact shock wave. Of many analytical models to predict the CIC test results, the empirical Jacobs–Roslund model [8] is notable which correlates the observed velocity thresholds with projectile diameter, nose shape, and thickness of the front cover at a given type of projectile material. Later semi-empirical one-dimensional models [9–11] additionally consider some shock variables (impact pressure, particle velocity, loading time, etc.) and have shown fair agreement to the experimental results.

Though the CIC test results have served as a useful parameter to describe the sensitivity of explosives, not all explosives in service have the geometry similar to the CIC test configuration. One good example is the ERA developed as a mass efficient way of protection method in many countries [12,13], in which thin explosive is encapsulated in a container material to form a cassette [14] for the convenience in manufacturing, storage, shipping and handling, and consideration of other engineering factors (see Fig. 1(b)). Since the operation of the armour system is triggered by a projectile impact, its sensitivity to the impact shock is an important factor in the design of overall armour system. As shown in Fig. 1(b), all surfaces of the explosive are confined in the cassette and the thickness of the explosive is in general far less than the lateral size while it is almost

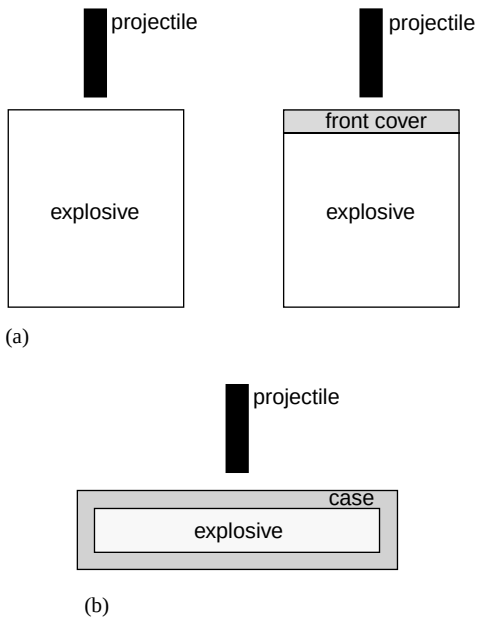

Fig. 1. Schematic diagram showing the difference in target geometry: (a) for a conventional explosive CIC test with and without front covers; and (b) for a reactive cassette impact test.

comparable to the lateral dimension in the conventional CIC target. Because of such difference in target geometry, an enough run-distance for a shock wave to detonate the thin confined explosive is questionable for various nose shapes of projectiles and therefore the use of CIC test results may not be suitable to establish the critical detonation condition of the reactive cassette. Hence, the validity of the previously established CIC results [4–8] and models [9–11] for many explosives has to be checked to determine whether they can be applied to the detonation criteria of a reactive cassette or not even though the cassette contains the same explosive.

In this respect, understanding physical phenomena associated with the detonation in a reactive cassette is of importance prior to either designing an impact test on the reactive cassette or interpreting the test results. Although an experimental approach offers the most accurate results, it is expensive and sometimes is practically difficult to perform an experiment. For instance, detonation behaviour of an explosive in a steel container (reactive cassette) is hardly visualized by the flash radiography technique. As an alternative approach, computational method can provide an insight which would be difficult to understand solely from the experimental data at a minimum cost. This work aims to numerically investigate the physical phenomena occurring in steel-encapsulated and doubly layered reactive cassettes by the impacts of projectiles. The detonation behaviour has been investigated for three different nose shapes of the projectile which can be practically encountered in an impact test, i.e., flat-ended, cone-nosed, and hemispherically nosed shapes.

2. Background

When a square shock pulse travels in a solid medium, the velocity of the release part of the shock (release wave) is faster than that of the front, since the release wave is traveling into a higher density material (already shocked and thereby compressed) than the shock front. Thus, the release wave eventually overtakes the shock front, resulting in a rapid decay of the shock pulse. In case a shock wave with a sufficient pressure travels in a solid heterogeneous explosive, it interacts with the density discontinuities in the explosive, producing numerous local hot spots behind the shock front [15,16]. Then a rapid chemical reaction takes place at the local hot spots. The chemical reaction, either governed by pressure [17] or rate of the grain burning [18], provides energy to the forward-moving shock front. In case the rate of the energy supply prevails on the effect of the release wave, the shock is prevented from decaying but reinforced until it detonates the explosive [19]. At detonation point, the chemical energy release-induced pressure wave overtakes and leads the shock front thereafter.

In numerical calculations on the shock wave interaction with an explosive, the formation of hot spots and the subsequent decomposition of the explosive for the pressure reinforcement are described by an evolutionary equation that has a number of empirical constants. In the forest fire model [17,20], which treats the shock as a simple plane wave [21], the gross feature of the process is modelled based on the experimental finding that the required run distance of a shock wave into an explosive for detonation is described as a function of initial shock pressure: a higher pressure shock requires a less run distance to detonate [22]. The reaction rate is thus given by a power series expansion of pressure [17,20]. Of the different approaches in setting up the evolutionary equation [23,24], the forest fire model has been incorporated in a number of one-, two-, and

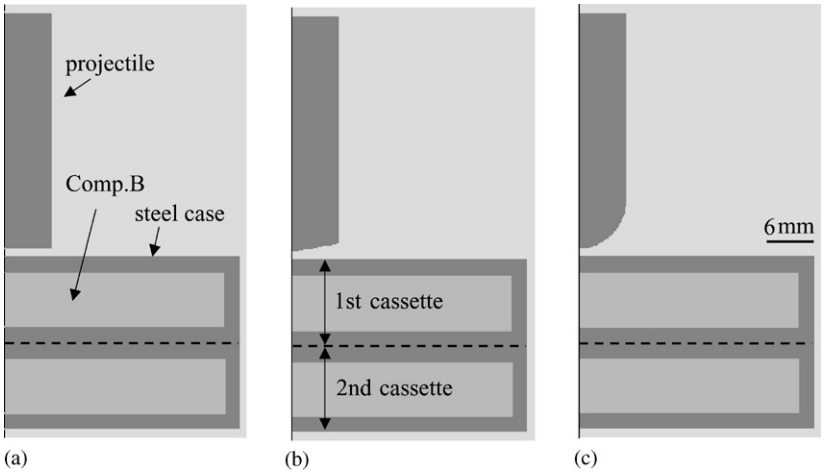

Fig. 2. Studied geometries of target and projectiles with: (a) a flat-ended nose; (b) a cone-shaped nose; and (c) a hemispherical nose.

three-dimensional hydrodynamic computer codes and has been applied to a variety of problems including corner turning at complicated geometries, failure diameter, retonation, etc. Its utility and predictive capability have been demonstrated and well documented [7,17,25–28]. The model is adopted in this work in order to investigate physical phenomena occurring when an impact shock travels in the geometrical situation of interest such as the reactive cassette.

3. Numerical analysis

The numerical analysis was performed using a finite difference hydrodynamic code Hull.[1] Since the lateral size of the reactive cassette is much larger than its thickness, the impact shock would reach the bottom of the cassette first and thus most of the detonation characteristics of the impacted cassette would be determined before the shock wave reaches the lateral end of the target. Hence the numerical analysis models for the cassette were simplified into two-dimensional axi-symmetric geometries for efficiency of numerical calculation as shown in Fig. 2. The basic analysis models in Fig. 2 consist of the cylindrical steel projectile, target structure, and surrounding air. The target consisted of two layers of disk-type reactive cassettes, each of which consists of an explosive disk (56 mm in diameter and 7 mm in thickness) encapsulated in a 2 mm thick steel case. The cylindrical steel projectiles were 30 mm in length and 12 mm in diameter with the impact velocity of 1800 m s^{-1}. The studied projectile parameter was its nose shape, i.e., flat-ended, conical (cone angle of 161.1°), and hemispherical shapes. The geometry for analysis in Fig. 2 was discretized using an Eulerian rectangular mesh (0.1 × 0.1 mm^2). In all the simulations, the initial tip positions of the projectiles were 1 mm away from the target surface and the direction of motion was toward the reactive cassette. The initial pressure of the air, projectile, case, and high

[1] Orlando Technology, Incorporated, Shalima, FL.

explosive was 1 atm (i.e., 101325 Pa), and this determined the state of the respective materials via the appropriate equation of state. No gravitational effect was considered in the simulation.

The condensed phase materials (projectile, case, explosive) were modelled using Mie–Gruneisen equation of state [29] with strength properties (except explosive), while the Jones–Wilkins–Lee [30] and gamma law equation of states [30] were used for the gaseous detonation product from the reactive material and air, respectively. As aforementioned, the forest fire reaction rate model [17,20] was adopted to describe the rate of energy release from the explosive, composition B, which is a mixture of about 55 wt% RDX,[2] and 45 wt% TNT.[3]

4. Results and discussions

4.1. Projectile with a flat-ended nose

Fig. 3 shows the detonation behaviour of the reactive cassette when impacted by a flat-nosed steel projectile. In the figure, areas representing material types are plotted on the right-hand side while pressure contour lines are on the left-hand side. Fig. 3(a) shows the generation of an impact shock pressure (about 42 GPa) at the front cover and projectile front. The generated shock pressure moves both upward and downward direction. At a later time step, as shown in Fig. 3(b), the high-pressure zone (the volume enclosed by the 40 GPa contour surface) has moved upward with respect to the cover plate/explosive interface. However, the pressure in the volume below the high-pressure zone has been decreased as compared with the previous time step. Such a pressure drop can be understood by considering the fact that the shock (compressive stress) wave travelling downward direction encounters the front cover/explosive interface beyond which the shock impedance, $K(=\rho_0 U_S$, where ρ_0 is density of material before shock compression and U_S is the velocity of shock wave) of the medium is lowered. In such a case, the reflected pressure from the interface has a tensile component resulting in the pressure drop, since particle velocity is accelerated as the wave trespasses the interface [31]. Such a zone in the cover plate eventually develops to a tensile region behind the high-pressure zone (Fig. 3(e)) and gap at later time steps (2–4.5 μs, e.g., Figs. 3(e) and (f)), followed by refilling of the gap by the incoming projectile after 4.5 μs (not shown in Fig. 3).

The pressure contour lines developed in the explosive in Fig. 3(b) indicates that only a part of the impact pressure is transmitted to the explosive (about 15 GPa as against 40 GPa). Based on a one-dimensional analysis [31], the ratio of incident to transmitted pressure across the interface is given in terms of shock impedance K,

$$\frac{P_T}{P_I} = \frac{2K_2}{K_2 + K_1}, \tag{1}$$

where P_T is the transmitted pressure, P_I is the incident pressure, and subscripts 1 and 2 denote steel case and explosive, respectively. Taking the shock velocity U_S as the elastic limit velocity (longitudinal sound velocity) for the steel case ($U_S = 4.6$ km s^{-1}, $\rho_0 = 7856$ kg m^{-3}) and explosive ($U_S = 2.9$ km s^{-1}, $\rho_0 = 1710$ kg m^{-3}) as a rough approximation, it is expected that

[2] No. X in Research Department explosive list (cyclotrimethylenetrinitramine).

[3] Trinitrotoluene.

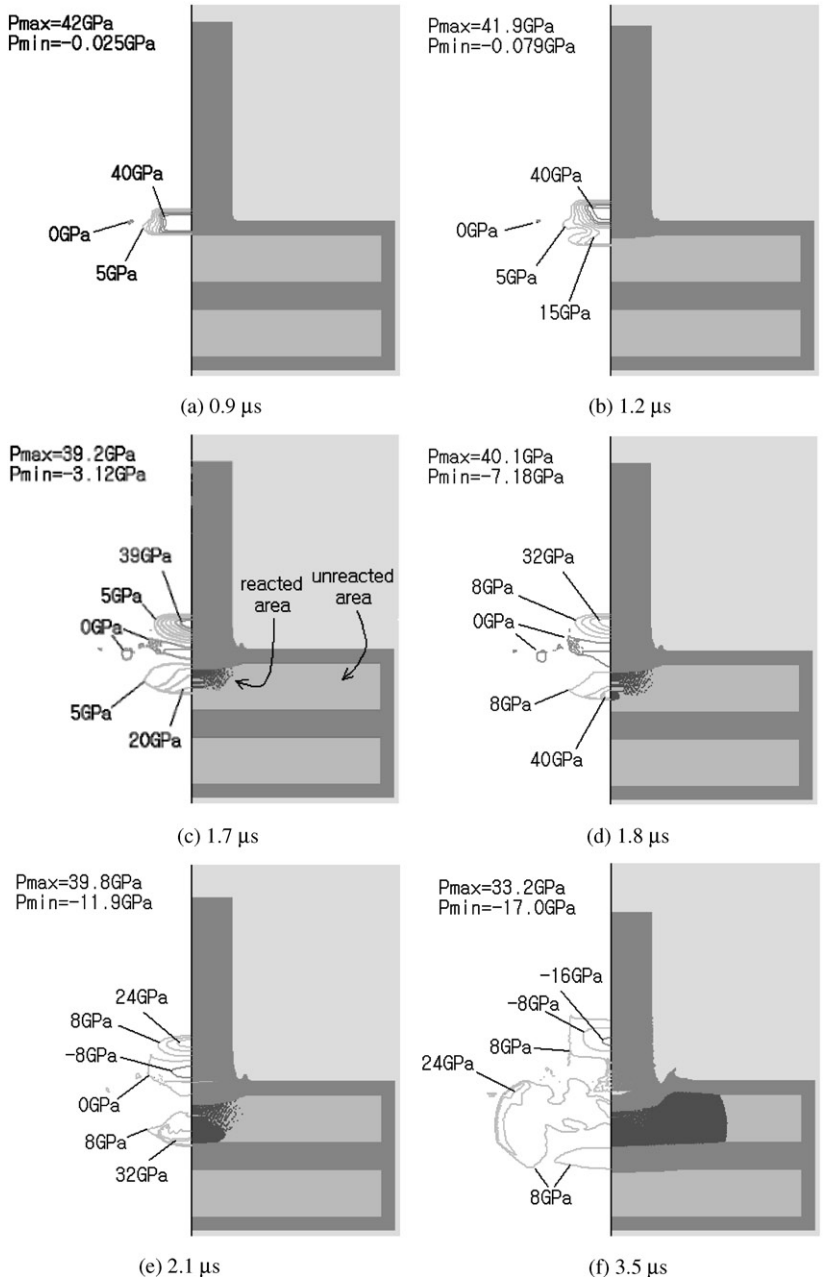

Fig. 3. Detonation behaviour of reactive cassettes at various time steps when impacted by a projectile with a flat-ended nose shape: (a) 0.9 μs; (b) 1.2 μs; (c) 1.7 μs; (d) 1.8 μs; (e) 2.1 μs; and (f) 3.5 μs.

about 24.1% of the impact pressure is transmitted to the explosive, i.e., 10.1 GPa. The pressure contour level in the explosive in Fig. 3(b) (about 15 GPa) is somewhat higher than this value. It is presumed that such difference arises from the use of the rough approximation in estimating the

shock velocity and also from the fact that the transmitted shock wave already progressed some distance into the explosive which accompanies some degree of pressure reinforcement process.

Fig. 3(c) shows the occurrence of the chemical reaction product (marked as reacted area in the figure) after the impact shock pressure travelled some distance (about 5 mm) into the reactive material. The chemical reaction product formed until 1.7 μs (Fig. 3(c)) is behind the shock front, implying that it could not develop to a detonation. This is due to the lack of run distance, as the forest fire model dictates. Note the newly appeared burn product area in Fig. 3(d) compared with Fig. 3(c), which appears in a small circular area inside the 40 GPa contour line. Now the newly appeared area is greatly reinforced in pressure (40.1 GPa) and its clear burn/un-burn interface leads the pressurized zone in a self-sustained mode at later time steps, e.g., in Figs. 3(e) and (f), implying that a detonation is occurring. Indeed, the same type of mechanism as the one occurring in the target geometry for the CIC test, i.e., the run distance-induced detonation is achieved even when the thin explosive is encapsulated in a steel case at the considered impact velocity (1800 m s^{-1}). If this is the case for all impact velocities, the threshold velocity determined by the reactive element test would be the same as the velocity obtained by the CIC test provided the same explosive and the front cover is used. However, this is not always the case as discussed in the next section.

In Fig. 3(f), the chemical reaction in the second reactive cassette is barely appreciable while the detonation in the first cassette progressed significantly. Actually, the detonation of the second (bottom) reactive cassette was triggered only after the full detonation of the first reactive cassette, so that a sufficient energy could be released from the first cassette (not shown here since a very similar result is presented in next section).

In general, a modified forest fire model is used for the cases when explosive detonation by a multiple shock loading is studied [20,32,33]. For instance, when a jet impacts onto a front-covered explosive, a forward-moving bow shock wave ahead of the jet tip pre-shocks the explosive meanwhile the jet penetrates into the front cover. In case the pre-shock is insufficient to detonate the explosive, it closes the hot spot sources such as voids, i.e., it makes the explosive more homogeneous. Then when the jet tip arrives at the explosive, the pre-shocked and thus desensitized explosive cannot be detonated by the impact of jet tip either. In order to properly simulate such a multiple shock phenomenon, the forest fire model is modified to add the Arrhenius decomposition rate law using local partially burned explosive temperature [20,32,33]. In the studied impact situation herein, however, the unmodified model has been used because this study investigates the interaction of the impact shock (a pre-shock) wave propagating well ahead of the slow- and large-diameter projectile (as compared with a jet) with the explosive in a cassette rather than the interaction of the slow-moving projectile tip with the pre-shocked explosive. In Fig. 3, indeed the un-reacted explosive at the location of detonation initiation receives a single shock (instead of multiple shock) before it detonates, i.e., detonation by the pre-shock takes place much before the slow-moving projectile arrives at the location of detonation.

4.2. Projectile with a conical nose

Fig. 4 shows the detonation behaviour of the reactive cassettes when impacted by a projectile with a conical nose shown in Fig. 2(b). Fig. 4(a) shows a significant initial formation of the chemical reaction product at the area impacted by the projectile tip, while such a burn product

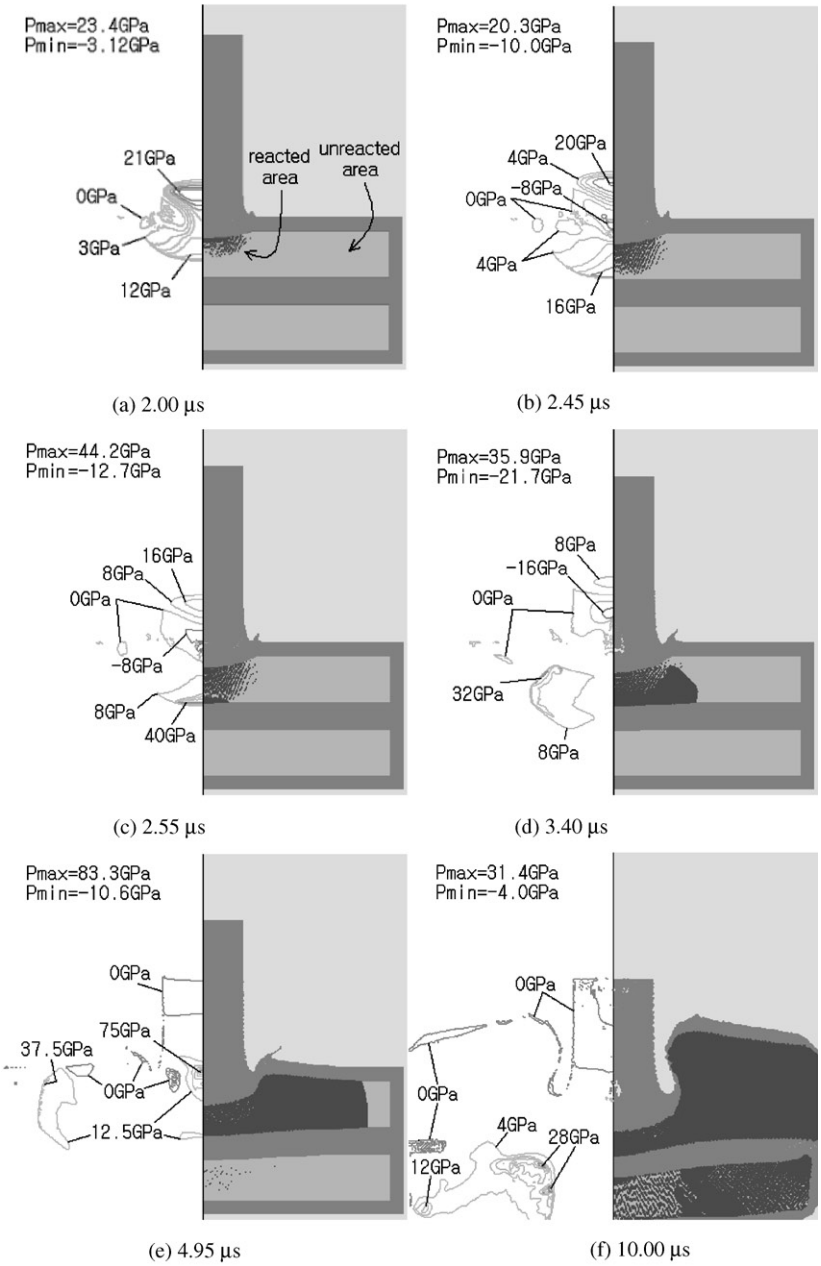

Fig. 4. Detonation behaviour of reactive cassettes at various time steps when impacted by a projectile with a cone-shaped nose: (a) 2.00 μs; (b) 2.45 μs; (c) 2.55 μs; (d) 3.40 μs; (e) 4.95 μs; and (f) 10.00 μs.

area does not lead the shock front. As can be seen in Fig. 4(b), the detonation does not seem to be achieved until the impact shock pressure wave almost reaches the bottom end of the first cassette. An apparent detonation takes place at the bottom of the reactive material in the first cassette after

the impact shock wave reached and reflected from the back plate (Fig. 4(c)) and the detonation propagates thereafter, e.g., in Figs. 4(d) and (e), to the un-reacted explosive area as well as the partially burned area (retonation).

The detonation at the bottom area of the first reactive cassette in Fig. 4 can be understood in the light of a one-dimensional analysis on the ratio of reflected to incident pressure at an interface of two different media [31]

$$\frac{P_R}{P_I} = \frac{K_2 - K_1}{K_2 + K_1}, \tag{2}$$

where P_R is the reflected pressure, P_I is the incident pressure, and subscripts 1 and 2 denote explosive and steel case, respectively. Taking appropriate values for the reactive materials and steel case as before gives the ratio of superposed pressure ($P_I + P_R$) to the incident pressure (P_I) of about 1.76. This implies that the shock pressure of the reactive material in the vicinity of the back plate is increased about 76% by the assistance of the presence of back plate. Thus, it is inferred that the detonation at the bottom area of the first reactive cassette is possible due to the superposition of incident and reflected shock waves by the presence of the back plate. The pressure reinforcement in the explosive area in contact with the back plate is achieved at the speed of shock wave which would be faster than any collapses of voids (which is performed at a much slower velocity of particle motions) for any desensitization in that area and thus the effect of the drastic pressure rise in that area would be a plausible source to increase the detonation sensitivity. Such a reinforcement mechanism can explain the increased detonation sensitivity of an explosive when it is confined by a high-impedance material as experimentally observed by Held [34]. Note that there has been a jump in the maximum pressure from about 16 (Fig. 4(b)) to 44 GPa (Fig. 4(c)) as the shock wave is reflected at bottom case, but the ratio of superposed pressure to incident pressure (2.75) much exceeds the result of one-dimensional analysis. The augmentation of pressure by the chemical reaction (detonation) counted in the simulation results would be mainly responsible for such a difference.

Fig. 4(e) shows that there is a merely appreciable chemical reaction product in the second reactive cassette while the detonation in the first cassette progressed significantly. The detonation of the second cassette is achieved at later time steps, e.g., 10 μs (Fig. 4(f)) after the detonation wave fully propagated in the first cassette. This means that the detonation of the second cassette is achieved by the energy release from the first cassette prior to the impact of the incoming projectile.

There has been no run distance-induced detonation for the case of the cone-nosed projectile (Fig. 4). However, when Figs. 4(a) and (b) are compared, the pressure of the shock front in the explosive in Fig. 4(b) (about 16 GPa) has been increased compared with that in former time step, i.e., in Fig. 4(a) (about 12 GPa). Thus, it may be argued that the cone-nosed projectile can also cause a run distance-induced detonation if a sufficient run distance for the shock wave is allowed, i.e., if the CIC target geometry is used. If the argument is valid, there may not be a difference between the two target geometries from the viewpoint that whether there is a detonation or not, even though the detonation mechanisms are obviously different for the two cases, i.e., back plate-assisted or run distance induced. Therefore, it is necessary to compare the detonation phenomena in Fig. 4 with those occurring in a CIC target geometry. Fig. 5 shows the simulation results when the target geometry has been changed to a CIC target configuration with an increased explosive thickness. As shown in the figure, the pressure of the shock front increases until 3.0 μs (about

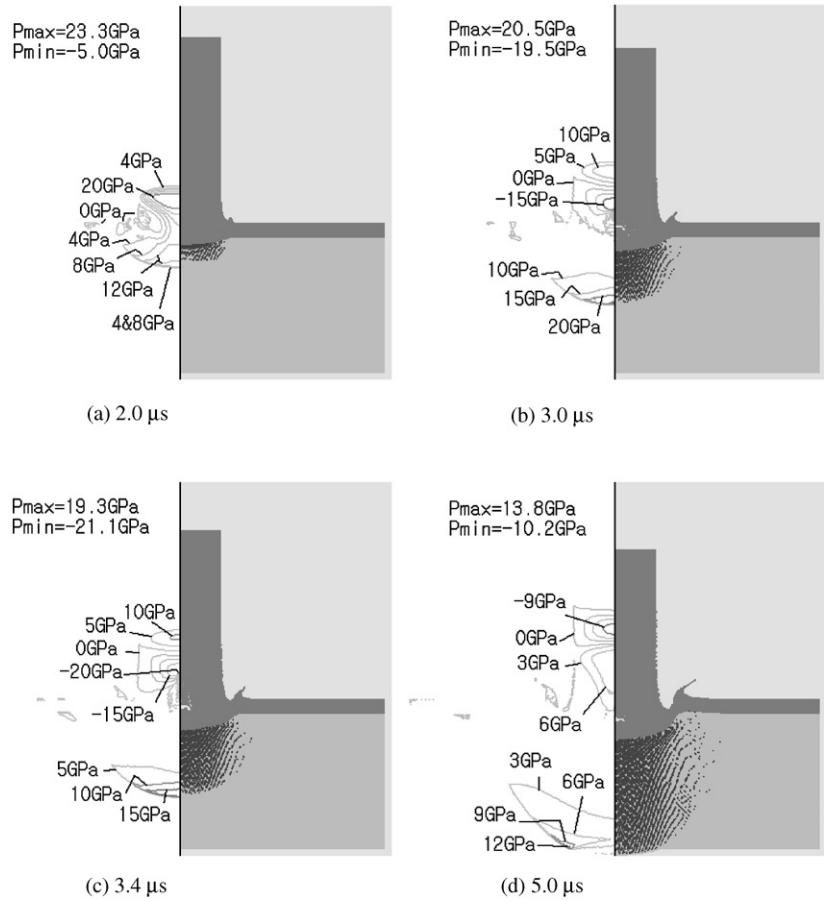

Fig. 5. Shock wave interactions in a CIC test target at various time steps when impacted by a projectile with a cone-shaped nose: (a) 2.0 μs; (b) 3.0 μs; (c) 3.4 μs; and (d) 5.0 μs.

20 GPa in Fig. 5(b)) but it decreases thereafter (about 15 and 12 GPa in Figs. 5(c) and (d), respectively). This implies that the effect of the release wave predominates over the provision of the chemical energy from the explosive decomposition. Thus, detonation in the CIC test configuration is certainly failed even though a sufficient run distance is allowed. Detonation in such a case certainly requires a higher impact velocity. Therefore, it is certain that the velocity threshold for detonation of an explosive is lowered when an explosive in a target geometry such as reactive cassette (Fig. 4) is impacted instead of a freely hanged explosive target without a rear confinement (Fig. 5). This indicates that, depending on the situations, the conventional CIC models for a given high explosive cannot be applied directly to predict the detonation condition of a reactive cassette. This necessitates the development of an extended analytical model for reactive cassette to include the additionally observed detonation mechanism.

Since the back plate-assisted mechanism is shown to be operative even when the run distance-induced detonation mechanism fails, it is necessary to check whether the same is true for the case of the flat-nosed projectile impact when the velocity is reduced. In a separate work, the impacts of

the flat-ended projectile on the two types of targets, i.e., CIC and reactive cassette targets, were simulated at 1700 m s^{-1}. The simulation results clearly indicated that the back plate-assisted detonation occurred in the reactive element target configuration while detonation failed in the CIC target geometry (not shown). This confirms above view that the reactive element target geometry yields a lower threshold velocity than the CIC test also for the case of an impact by a flat-nosed projectile.

4.3. Projectile with a hemispherical nose

Fig. 6 shows the impact behaviour of the reactive cassette target by a projectile with a hemispherical nose. As shown in Fig. 6(a), the superposition of the incident and reflected shock pressure waves at the explosive/back plate interface region is apparent but the pressure level is only about 5 GPa, which is far less than the pressure level in the cone-nosed case (Fig. 5(b)). At a later time step in Fig. 6(c), the squeezing out of the reactive material from the central axis (high-pressure region between projectile and the back plate) yields a further increase in pressure while not resulting in the detonation. The failure of detonation in the hemispherically nosed case in

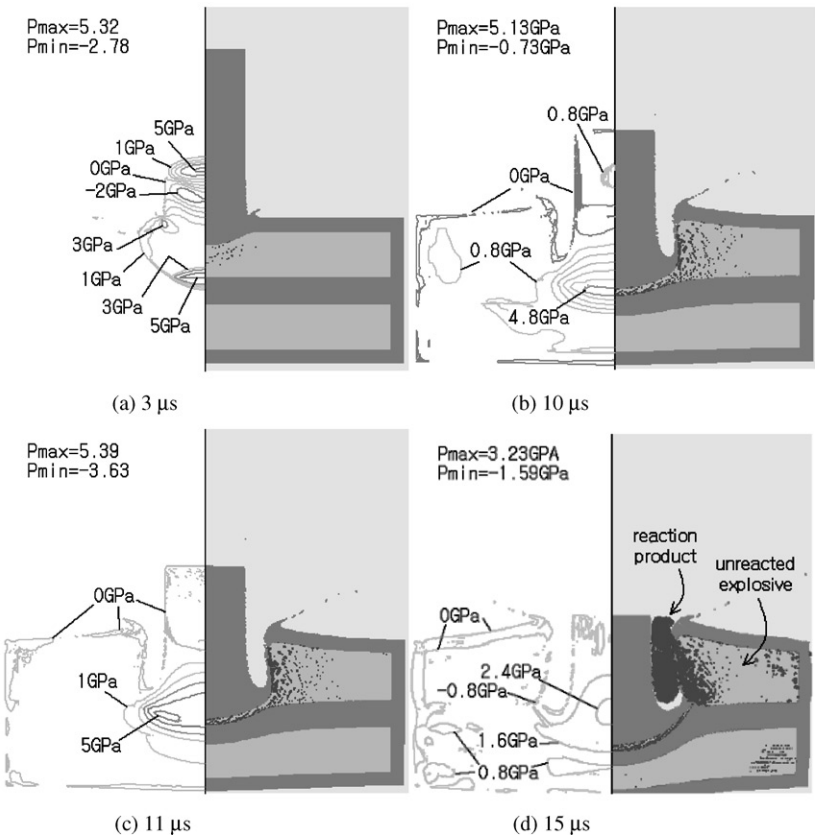

Fig. 6. Shock wave interactions in reactive cassettes at various time steps when impacted by a projectile with a hemispherical nose shape: (a) 3 μs; (b) 10 μs; (c) 11 μs; and (d) 15 μs.

Fig. 6 is consistent with the experimental finding that the threshold impact velocity for a hemispherically nosed projectile increases drastically compared with that for a flat-ended one [6–8]. The failure of detonation in the first cassette subsequently led to the failure of the detonation in the second cassette at later time steps (not shown in Fig. 6). Since the previous two cases, i.e., the flat-ended and conical noses, resulted in the detonation of the second cassette following that of the first one, it is inferred that the second cassette detonates only when the first cassette fully detonates thereby releasing sufficient energy to the second one.

5. Summary

The detonation behaviours of doubly layered reactive cassettes, the geometry of which is considerably different from conventional CIC test targets, have been investigated numerically for the cases of the impacts by steel projectiles with different nose shapes. When a flat-ended projectile impacted the reactive cassette at 1800 m s^{-1}, a run distance-induced detonation was predicted to occur as in the case of a CIC test. However, this was not the case when the target was impacted with a cone-nosed projectile at the same velocity or when the flat-ended projectile impacted at a lower velocity, namely 1700 m s^{-1}. In such cases, though the run distance-induced detonation failed, detonation of the explosive target was achieved via the back plate-assisted shock reinforcement mechanism. Analysis on these two cases was extended to the case of CIC test geometry, but no detonation occurred even though an enough run distance was allowed. Since the back plate-assisted detonation mechanism in above cases operates even when the run distance-induced detonation fails, the threshold velocity of detonation determined by the reactive cassette test is expected to be lower than that by the CIC test where no back plates are present, indicating that CIC test result alone may not be sufficient to evaluate the response reliability of confined explosives.

When the projectile with a hemispherical nose impacted the target, the back plate-assisted pressure build-up was followed by a squeezing out action of the pressurized reactive material from the path of the penetrator. However, such phenomena could not result in detonation since the pressure build-up itself was insufficient. In this case, detonation of the second reactive cassette failed to occur whereas detonation of the first cassette accompanied the detonation of the second cassette in the previous two cases of flat-nose and cone-nose projectile impacts. These results imply that the detonation of the second reactive cassette is not directly influenced by the impact shock of all the considered projectiles. Instead, it is triggered by the transfer of sufficient energy released from the full detonation of the first cassette.

References

[1] Naval Surface Warfare Center. Hazard assessment tests for non-nuclear munitions. Military Standard No. MIL-STD-2105B, Department of Defense, Indian Head, MD, 1994.
[2] Held M. Initiation of covered high explosives has many facettes. Proceedings of the Third European Armoured Fighting Vehicle Symposium, Shrivenham, UK, 1998.
[3] US Army Test and Evaluation Command. Typical reactive armor safety tests. Test Operations Procedure No. TOP-2-2-623. Army Research Laboratory, Aberdeen Proving Ground, Maryland, USA, 1993.

[4] Griffiths N, Laider RM, Spooner ST. Some aspects of the shock initiation of condensed explosives. Combust Flame 1963;7:347–52.
[5] Eldh D, Persson B, Ohlin B, Johansson CH, Ljungberg S, Sjolin T. Shooting test with plane impact surface for determining the sensitivity of explosives. Explosivstoffe 1963;5:97–103.
[6] Bahl KL, Vantine HC, Weingart RC. The shock initiation of bare and covered explosives by projectile impact. Proceedings of the Seventh International Symposium on Detonation, Office of Naval Research, Arlington, VA, USA, 1981. p. 325–35.
[7] Borg RAJ, Jones DA. Numerical simulation of projectile impact experiments using the forest fire reaction rate model. Report No. DSTO-TR-0325. Defence Science and Technology Organisation, Canberra, Australia, 1996.
[8] Roslund LA, Watt JM, Coleburn NL. Initiation of warhead explosives by the impact of controlled fragments in normal impact. Report No. NOLTR 73-124. Naval Ordnance Laboratory, White Oak, MA, USA, 1975.
[9] James HR. Critical energy criterion for the shock initiation of explosives by projectile impact. Propellants Explos Pyrotech 1988;13:35–41.
[10] Billingsley JP, Adams CL. Remarks on certain aspects of solid explosive detonation via small projectile impact. Technical Report No. RD-SS-88-11. US Army Missile Command, Redstone Arsenal, Alabama, USA, 1989.
[11] James HR, Haskins PJ, Cook MD. An extension to the critical energy criterion used to predict shock initiation thresholds. Propellants Explos Pyrotech 1996;21:251–7.
[12] Foss CF. China develops its own reactive armour family. Jane's Defence Weekly 1997;7 May:15.
[13] Foss CF. RFAS explosive reactive armour. Jane's Armour and Artillery Upgrades 2000–2001, 21 September, 2000.
[14] Held M. Protective arrangement against projectiles, particularly hollow explosive charges. US patent No. 4,368,660, 1983.
[15] Johansson CH, Persson PA. Detonics of high explosives. London: Academic Press, 1970.
[16] Langer G, Eisenreich N. Hot spots in energetic materials. Propellants Explos Pyrotech 1999;24:113–8.
[17] Mader CL. Numerical modelling of explosives and propellants, 2nd ed. New York: CRC Press, 1998.
[18] Howe P, Frey R, Taylor B, Boyle V. Shock initiation and critical area concept. Proceedings of the Sixth International Symposium on Detonation. Office of Naval Research, Arlington, VA, USA, 1976. p. 11–9.
[19] Cooper PW, Kurowski SR. Introduction to the technology of explosive. New York: VCH Publishers Inc., 1996.
[20] Mader CL, Forest CA. Two-dimensional homogeneous and heterogeneous detonation wave propagation. Report No. LA-6259. Los Alamos Scientific Laboratory, Los Alamos, NM, USA, 1976.
[21] Leiber C-O. Physical model of explosion phenomena—physical substantiation of Kamlet's complaint. Propellants Explos Pyrotech 2001;26:302–10.
[22] Ramsay JB, Popolato A. Analysis of shock wave and initiation data for solid explosives. Proceedings of the Fourth International Symposium on Detonation. Office of Naval Research, Arlington, VA, USA, 1965. p. 233–8.
[23] Lee EL, Tarver CM. Phenomenological model of shock initiation in heterogeneous explosives. Phys Fluids 1980;23:2362–72.
[24] James HR, Lambourn BD. A continuum based reaction growth model for the shock initiation of explosive. Propellants Explos Pyrotech 2001;26:246–56.
[25] Lundstrom EA. Evaluation of forest fire burn model of reaction kinetics of heterogeneous explosives. Report No. NWC-TP-6898. Naval Weapons Center, China Lake, CA, USA, 1988.
[26] Lawrence W, Starkenberg J. The effects of the failure diameter of an explosive on its response to shaped charge jet attack. Report No. ARL-TR-1350. Army Research Laboratory, Aberdeen Proving Ground, Maryland, USA, 1997.
[27] Chou PC, Liang D, Flis WJ. Shock and shear initiation of explosive. Shock Waves 1991;1:285–92.
[28] Chou PC, Roslund L, Liang D. Impact initiated annular retonation wave in explosive. Propellants Explos Pyrotech 1993;18:264–9.
[29] Bakken LH, Anderson PD. An equation of state handbook. Report No. SCL-DR-68-123. Sandia National Laboratory, Albuquerque, NM, USA, 1969.
[30] Lee EL, Finger M, Collins W. JWL equation of state coefficients for high explosives. Report No. UCID-16189. Lawrence Radiation Laboratory, University of California, Livermore, CA, USA, 1973.

[31] Meyers MA. Dynamic behaviour of materials. New York: Wiley, 1994.
[32] Chick MC, Hatt DJ. The mechanism of initiation of composition B by a metal jet. Proceedings of the Seventh International Symposium on Detonation. Office of Naval Research, Arlington, VA, USA, 1981. p. 352-61.
[33] Chick MC, MacIntyre IB. The jet initiation of solid explosives. Proceedings of the Eighth International Symposium on Detonation. Office of Naval Research, Arlington, VA, USA, 1985. p. 318–27.
[34] Held M. Reaction thresholds in unconfined and confined charges by shock load. Propellants Explos Pyrotech 2000;25:107–11.